energies

MDPI

Article

Influence of Copper and Tin Oxidation States on the Phase Evolution of Solution-Processed Ag-Alloyed CZTS Photovoltaic Absorbers

Abdeljalil Errafyg [1,2], Naoufal Ennouhi [1,2], Yassine Chouimi [2] and Zouheir Sekkat [1,2,*]

[1] Department of Chemistry, Faculty of Sciences, Mohammed V University, Rabat 10000, Morocco
[2] Optics and Photonics Center, Moroccan Foundation for Advanced Science & Innovation & Research, MAScIR-UM6P, Benguerir 43150, Morocco
* Correspondence: z.sekkat@um5r.ac.ma

Abstract: Kesterite-based semiconductors, particularly copper–zinc–tin–sulfide (CZTS), have garnered considerable attention as potential absorber layers in thin-film solar cells because of their abundance, nontoxicity, and cost-effectiveness. In this study, we explored the synthesis of Ag-alloyed CZTS (ACZTS) materials via the sol–gel method and deposited them on a transparent fluorine-doped tin oxide (FTO) back electrode. A key challenge is the selection and manipulation of metal–salt precursors, with a particular focus on the oxidation states of copper (Cu) and tin (Sn) ions. Two distinct protocols, varying the oxidation states of the Cu and Sn ions, were employed to synthesize the ACZTS materials. The transfer from the solution to the precursor film was analyzed, followed by annealing at different temperatures under a sulfur atmosphere to investigate the behavior and growth of these materials during the final stage of annealing. Our results show that the precursor transformation from solution to film is highly sensitive to the oxidation states of these metal ions, significantly influencing the chemical reactions during sol–gel synthesis and subsequent annealing. Furthermore, the formation pathway of the kesterite phase at elevated temperatures differs between the two protocols. Structural, morphological, and optical properties were characterized via X-ray diffraction (XRD), Raman spectroscopy, and scanning electron microscopy (SEM). Our findings highlight the critical role of the Cu and Sn oxidation states in the formation of high-quality kesterite materials. Additionally, we studied a novel approach for controlling the synthesis and phase evolution of kesterite materials via molecular inks, which could provide new opportunities for enhancing the efficiency of thin-film solar cells.

Keywords: kesterite; ACZTS; sol–gel; solar cells

Citation: Errafyg, A.; Ennouhi, N.; Chouimi, Y.; Sekkat, Z. Influence of Copper and Tin Oxidation States on the Phase Evolution of Solution-Processed Ag-Alloyed CZTS Photovoltaic Absorbers. *Energies* **2024**, *17*, 6341. https://doi.org/10.3390/en17246341

Academic Editor: Andrea Reale

Received: 25 October 2024
Revised: 29 November 2024
Accepted: 9 December 2024
Published: 17 December 2024

1. Introduction

Recently, there has been significant interest in materials belonging to the kesterite family, which are attracting attention as promising semiconductors for use as absorber layers in thin-film solar cells. Kesterite materials shows opto-electronic properties similar to those reported in other thin-film technologies used in photovoltaic application such as nano-structure based on CdTe and GaAS materials [1–3]. However, the toxicity of cadmium in CdTe and the rarerty of Ga in GaAs attract more researchers to work on kesterite absorber which is based on low-cost and non-toxic elements. Recent advancements in CZTS thin-film and mono-grain technologies have demonstrated their potential for practical applications, with minimal efficiency losses observed during long-term stability tests under indoor and outdoor conditions. Scalable deposition methods, such as colloidal ink spraying and spin coating, have shown promising results, achieving efficiencies above 7% in early large-area tests. These developments suggest that kesterite-based solar cells could be viable for photovoltaic applications, leveraging their suitability for mass production. However, challenges related to phase purity, efficiency, and integration into industrial processes must

still be addressed to fully realize their potential [4]. In this fact, various efforts have been made to develop high-quality kesterite absorbers through both physical and chemical approaches [5–8]. Among these approaches, solution deposition methods, such as the sol–gel technique, are widely preferred because of their convenience and cost-effectiveness. As of 2012, the efficiency of kesterite-based solar cells reached approximately 12.6% [9], with the absorbers in these solar cells being fabricated via the sol–gel method. Since then, numerous studies have focused on enhancing the performance of kesterite-based solar cells via advanced deposition techniques. However, in 2023, the highest reported efficiency of up to 14% was achieved via spin-coated ACZTSSe absorbers [10], highlighting the potential of sol–gel methods for developing highly efficient kesterite solar cells. However, it is worth noting that the preparation of kesterite materials via the sol–gel method is quite complicated compared to that of physical methods (e.g., PVD). This process involves several steps, including solution preparation, deposition, and annealing, all of which must be optimized to achieve the desired quality of absorbers. Unlike physical deposition approaches, which utilize metal- or chalcogen-containing precursors subjected to annealing [11], the sol–gel method requires the use of metal salt precursors dissolved in organic solvents, which may contain additional elements. Despite this complexity, a diverse range of metal precursor salts (e.g., acetate, nitrate, sulfate, and chloride) and solvents can be employed in kesterite synthesis via the sol–gel method. Consequently, numerous studies have been conducted to identify the optimal precursor salts and solvents for this purpose [12,13]. As the sol–gel reaction process is designed to produce organic products that can fully evaporate during the high-temperature stage used in CZTS fabrication, the oxidation state of the metal salt used in the solution can be an important factor in controlling the phase evolution of CZTS materials. However, few studies have reported the influence of the oxidation state of the metal precursors used during CZTS preparation with sol–gel methods, especially copper (Cu) and tin (Sn), and all these works support the significant effect of the metal ions oxidation state on the properties of CZTSSe absorbers [14–17].

The most used protocol for preparing CZTS solutions involves Cu^{2+} and Sn^{2+} metal precursors, where an oxidoreduction reaction determines the final CZTS material properties [18]. This approach has enabled efficiencies up to 12.6% for CZTSSe solar cells [9]. More recently, a 12.4% efficiency was achieved using Cu^{+} and Sn^{4+} precursors, demonstrating the potential of this method when combined with innovations like silver alloying and controlled selenium vapor pressure during annealing [17].

The transition from solution to substrate significantly impacts the phase composition of the precursor, which is crucial during the annealing process. While physical deposition methods utilize various precursors with distinct growth mechanisms, sol–gel methods primarily control precursor phase composition through the oxidation states of metal ions, offering great potential for kesterite solar cell development. However, most research has focused on narrow-bandgap sulfo-selenide compounds, with limited attention to large-bandgap sulfide compounds (CZTS), which are essential for tandem applications.

Recently, kesterite materials have achieved improved performance by introducing silver alloying for the sulfo-selinide compounds ACZTSSe on transparent substrates, and these approaches can lead to the enhancement of large-bandgap pure sulfide kesterite CZTS, which is essential for developing semitransparent or tandem solar cells.

The majority of studies on large-bandgap CZTS-based solar cells prepared using the sol–gel method have primarily focused on two critical aspects: the deposition of precursor thin films and the subsequent annealing process. However, there is a notable absence in the existing literature regarding a comprehensive examination of the solution phase, which is of paramount importance in determining the quality of the final absorber layer. While some attempts have been made to study the influence of metal–salt precursors and the choice of solvents [19], it is notable that the oxidation state of the metal ions in the solution phase, to the best of our knowledge, has not been systematically reported for CZTS absorbers. This oversight is notable, as the oxidation state of metal ions is a critical factor in controlling phase evolution during synthesis. Studies on narrow-bandgap CZTSSe absorbers have

demonstrated that tailoring the oxidation state of the metal ions can significantly enhance the performance of the final solar cell [20]. Therefore, extending this approach to large-bandgap CZTS absorbers could provide valuable insights and potentially lead to improved device efficiency.

In this study, we investigated how different oxidation states of Sn and Cu during ACZTS ($AgCu_2ZnSnS_4$) solution preparation impact the transformation from solution to solid precursors and the behavior of the final ACZTS absorbers during high-temperature sulfurization. CZTS sol–gel solutions were prepared via two protocols involving Sn^{2+} + Cu^{2+} and Sn^{4+} + Cu^{1+} combinations, which are widely reported in kesterite research. The as-deposited ACZTS precursors from both protocols were analyzed, and the transition from solution to precursor was examined. Additionally, the phase evolution during high-temperature annealing under a sulfur atmosphere was investigated via various characterization methods.

2. Materials and Methods

2.1. Preparation of the ACZTS Sol–Gel Solution

Solid-solution ACZTS materials were synthesized via the cost-effective sol–gel method via 2 protocols with different Sn and Cu oxidation states. All chemicals used in this study were purchased from Sigma-Aldrich(is an American chemical, life science, and biotechnology company owned by the multinational chemical conglomerate Merck Group, Saint-Louis, MO, USA) with a purity of 99.9%

Protocol 1: Initially, $Cu(CH_3COO)_2{\cdot}H_2O$ + AgCl (0.46 mol/L) was dissolved in 20 mL of 2-methoxyethanol, followed by the addition of SnCl2-2H2O (0.27 mol/L). Then, $Zn(CH_3COO)_2{\cdot}2H_2O$ (0.27 mol/L) and thiourea $SC(NH_2)_2$ (2 mol/L) were added, resulting in a transparent solution, and the entire solution was stirred for one hour at 60 °C, yielding a clear and transparent solution. NaCl:H_2O was then added to the final CZTS solution until a NaCl:CZTS molar ratios of up to 10% was reached.

Protocol 2: ACZTS Solution 2 was synthesized employing copper chloride (CuCl) + Silver chloride AgCl (0.46 mol/L), zinc acetate dihydrate (Zn $(CH_3COO)2{\cdot}2H_2O$) (0.27 mol/L), tin(IV) chloride ($SnCl_4$) (0.27 mol/L), and thiourea ($SC(NH_2)_2$) (2 mol/L) as the metal and sulfur sources. However, following a similar process as that reported in [12], 2-methoxyethanol was used as a solvent instead of DMSO. Two separate solutions were prepared:

For Solution 1, thiourea ($SC(NH_2)_2$) and CuCl + AgCl were dissolved in 2-methoxyethanol. For Solution 2, $SnCl_4$ was dissolved in 2-methoxyethanol, followed by $Zn(CH_3COO)_2{\cdot}2\ H_2O$, maintaining a Zn/Sn ratio of 1.1 and a Cu/(Sn + Zn) ratio of 0.75.

Both solutions were stirred for 24 h to ensure complete dissolution of the metal–salt precursors. The solutions were subsequently mixed and stirred at 60 °C for 1 h in an oil bath.

2.2. Chemical Reactions

In a non-aqueous sol–gel synthesis of kesterite absorbers, metal salts react with thiourea (Tu) in the presence of an alcohol, in this case 2-methoxyethanol.

This reaction process occurred during the sol–gel solution preparation and begins with the formation of thiourea–metal complexes.

The general steps and reactions are as follows [21]:

One-Complex Formation (Equation (1)): metal ions (M) such as Cu^{2+}, Zn^{2+}, and Sn^{2+} react with thiourea (Tu) to form thiourea–metal complexes:

$$M - X + Tu \rightarrow [M(Tu)m] - X \quad (1)$$

where M represents metal ions (Cu, Zn, and Sn); X represents anions (such as CH_3COO^- or Cl^-), and [M(Tu)m] − X represents the thiourea–metal complex.

Two-Alcoholysis and Condensation Reactions (Equations (2) and (3)):

The thiourea–metal complex undergoes alcoholysis with 2-methoxyethanol (ROH):

$$[M(Tu)m] - X + ROH \rightarrow [M(Tu)m] - OR + H - X \quad (2)$$

This reaction produces an intermediate complex with an organic chain attached $M(Tu)m] - OR$ and a byproduct acid $(H - X)$.

The resulting complexes then undergo polycondensation:

$$[M(Tu)m] - X + [M(Tu)m] - OR \rightarrow [M(Tu)m] - O - [M(Tu)m] + R - X \quad (3)$$

In this step, complexes link together through an oxygen bridge, resulting in the formation of nanoparticles. Then, during the deposition process, these complexes lead to sulfide formation and volatile byproducts.

2.3. Deposition Process

Prior to deposition, the FTO-coated soda lime glass (SLG) substrate (surface resistivity of ~7 Ω/sq) underwent a thorough cleaning process in an ultrasonic bath, followed by UV–ozone cleaning for 10 min. The filtered solution (through a 0.45 µm filter) was deposited onto the cleaned FTO substrate via spin-coating at 3000 rpm for 30 s. The substrate was subsequently preheated in an atmospheric environment on a hot plate set at 300 °C for 2 min. This deposition process was repeated 7 times to achieve the desired thickness.

2.4. Sulfurization Process

The as-deposited ACZTS precursors were placed in a graphite box (4×5 cm^2) with 500 mg of sulfur powder and inserted into a tubular furnace. Prior to the annealing process, the tube was purged several times with nitrogen. The sulfurization process was conducted at temperatures ranging from 475 to 550 °C for 30 min under a pressure of approximately 1 bar (initially 600 mbar at 25 °C). The ramping rate was set to 5 °C/min, and the cooling process occurred naturally over approximately 3 h. The annealing conditions employed in this study were determined based on previous optimization studies. The final optimized annealing profile, utilized to achieve the best results, is presented in Figure 1.

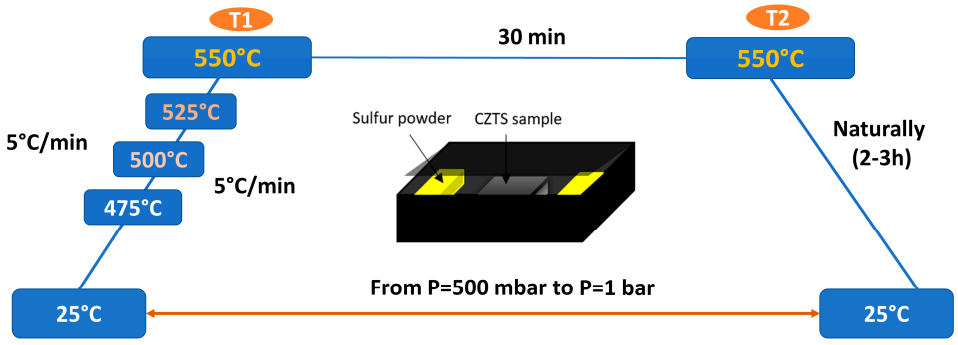

Figure 1. The optimized annealing profile used in this work.

2.5. Characterizations

Scanning electron microscopy (SEM) images were acquired via an FEI FEG 450 (field emission gun) (Europe Research Center, Palaiseau, France) microscope with an acceleration voltage of 5 kV. X-ray diffraction (XRD) patterns were collected using a Rigaku SmartLab diffractometer (Rigaku SmartLab, Tokyo, Japen) in Bragg–Brentano geometry. A graphite monochromator was used with a CuKα source (λ = 1.54178 Å), representing the average wavelength of the Cu Kα1,2 doublet, and the detector was a D/teX Ultra 250 1D silicon strip detector. Raman spectroscopy was conducted using a LabRam Aramis microprobe by Horiba Jobin-Yvon Co. (Edison, NJ, USA) with 532 and 785 nm excitation to study the structural properties and assess the quality of the ACZTS films.

3. Results

3.1. From Solution to Precursor Transfer

One of the critical steps in CZTS preparation via the sol–gel method is the transition from the solution to the precursor, which is typically achieved through spin-coating techniques followed by preheating at temperatures ranging between 250 and 300 °C [19]. In previous studies that utilized DMSO as a solvent, the as-deposited precursors from a solution containing Cu^{1+} and Sn^{4+} resulted in the formation of an amorphous CZTS phase, whereas binary phases tended to dominate in the as-deposited solution containing Cu^{1+} and Sn^{2+} [22]. In this work, the Cu^{2+} and Sn^{2+} used in Sol-1 serve as sources of Cu and Sn, with Sn^{2+} eventually transforming into the necessary Sn^{4+} for kesterite materials. This transformation occurs through oxidoreduction reactions of Cu and Sn, as depicted in Equation (1). Moreover, the remaining Sn^{2+} due to the Cu-poor stoichiometry and nonideal oxidoreduction reactions promoted the formation of SnS phases and ZnS phases. On the other hand, the use of Sn^{4+} and Cu^{+} in Sol-2 can directly facilitate the formation of kesterite phases following preheating.

To explore the disparities between the two protocols, we conducted XRD and Raman analyses on the as-deposited Sol-1 and Sol-2 samples, which are referred to as Prec-1 and Prec-2, respectively. Figure 2 displays the XRD patterns of the ACZTS precursors deposited from Sol-1 and Sol-2. Both samples exhibit a broad diffraction peak attributed to the kesterite phase (JCPDS # 026--0575), with the broadness and asymmetry of the peaks indicating the formation of an amorphous kesterite structure, which is consistent with previous reports on spin-coated CZTS solutions [23]. However, the shape and intensity of the main diffraction peak corresponding to the (112) orientation differ between the two samples. The peak in sample Prec-2 is narrower and more intense than that in Prec-1, suggesting that a greater quantity of the kesterite phase forms in Prec-2, where the ions are in the oxidation states required for CZTS formation. In contrast, Sol-1 appears to undergo redox reactions that convert the Sn and Cu ions to the necessary oxidation states, complicating the formation of the kesterite phase in these precursors and promoting the formation of secondary phases during the preheating stage. A similar trend was observed in the Raman spectra of the as-deposited CZTS precursors (Figure 3b), which were obtained with 785 nm excitation. Both samples display a broad peak between 250 and 400 cm^{-1}, encompassing the main vibrational modes associated with the S–S bonds in the kesterite structure [24]. However, the peaks in the sample prepared from Sol-2 are narrower and more symmetric, indicating that the quantity of the kesterite phase is greater than that in the sample prepared from Sol-1. In the Raman spectra obtained via 532 nm (Figure 3a) excitation for Prec-1, some traces of Cu_2-xS and SnS_2 were observed; however, in Prec-2, no secondary phases were detected, indicating the formation of an amorphous ACZTS phase after the preheating process.

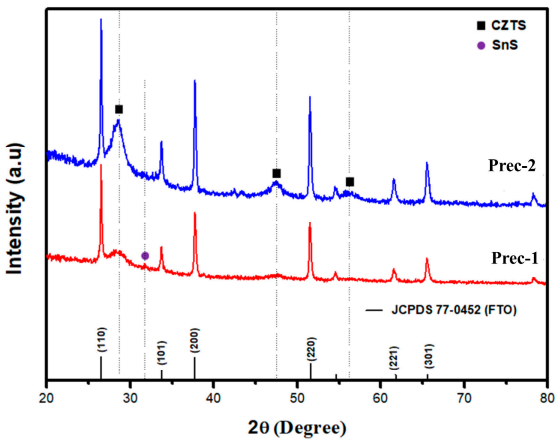

Figure 2. XRD patterns of ACZTS precursors deposited from Sol-1 or Sol-2.

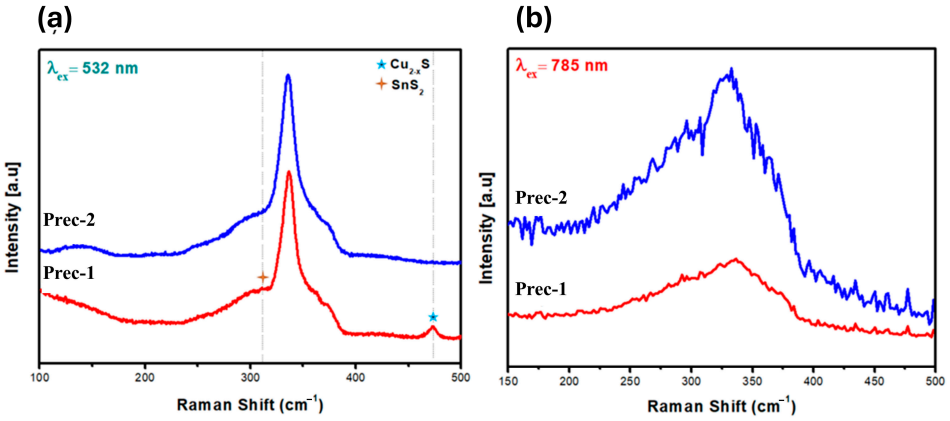

Figure 3. Raman s spectra of CZTS precursors deposited from Sol-1 or Sol-2, recorded with excitation wavelengths of 532 (**a**) and 785 nm (**b**).

Despite all the samples having similar concentrations of metal precursors, this discrepancy can be attributed to the differences in the oxidation states of Sn and Cu in the solutions. In Sol-2, the Sn and Cu ions are already in the appropriate oxidation states for kesterite formation, facilitating the development of the kesterite phase at the lower preheating temperature of 300 °C. In contrast, Sol-1 requires the conversion of Sn^{2+} to Sn^{4+} (Equation (4)). The incomplete oxidation of Sn results in a significant fraction of Sn remaining in the 2+ state, leading to the formation of the SnS binary phase, which is evidenced by the intense peak at 31.57° in the XRD pattern corresponding to the (100) orientation [25]. Additionally, Cu ions in the necessary oxidation state promote the formation of the Cu_2S binary phase. The presence of both SnS and Cu_2S suggests the coexistence of ZnS due to the Zn-rich composition, although ZnS cannot be clearly distinguished from CZTS because of peak overlap in the diffraction patterns [26]. These findings highlight the crucial role of the oxidation states of Sn and Cu in determining the phases present in the CZTS precursors. Importantly, the mechanism by which CZTS absorbers form during annealing is strongly influenced by the initial precursor phases and composition.

$$Sn^{2+} + 2Cu^{2+} = Sn^{4+} + 2Cu^{+} \quad (4)$$

The previous results highlighted the significant impact of the oxidation states of Sn and Cu on the phase compositions of CZTS precursors. Figure 4 illustrates the transformation mechanisms from solution to precursor for the three different protocols. In Sol-2 (Sn^{4+} + Cu^{1+}), where Cu and Sn ions already have the oxidation states required for kesterite formation, CZTS nanoparticles are formed during the polycondensation process. During the preheating step, these CZTS nanoparticles directly transform into an amorphous CZTS phase. In Sol-1, both Sn^{2+} and Cu^{2+} need to be converted to Cu^{1+} and Sn^{4+}. This transformation involves redox reactions between Cu and Sn, as well as redox reactions of Sn with oxygen. A significant amount of Sn and Cu ions are converted, forming CZTS nanoparticles. However, some ions remain in their initial oxidation states, leading to the formation of the CuS, SnS, and ZnS phases in the precursors. These observations underscore the critical role of oxidation state management in determining the phase composition and quality of CZTS precursors, which in turn affects the main properties of the final CZTS absorbers.

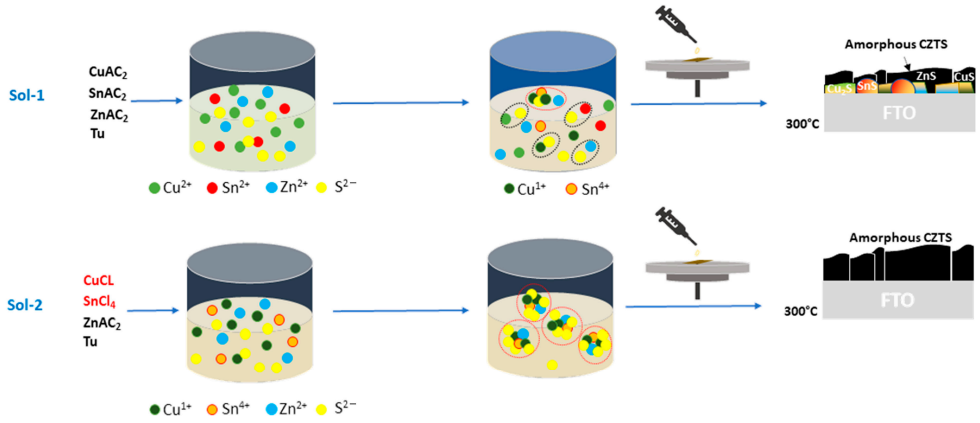

Figure 4. Transformation mechanisms from solution to precursor for the two different protocols.

3.2. From Precursor to Absorber Transfer

During the annealing process, kesterite formation typically occurs at lower temperatures, where various phases melt and interact with the chalcogens (S and/or Se) present in the atmosphere. At higher temperatures, the kesterite phase becomes dominant, promoting improved crystallinity and grain growth in CZTS materials [27]. The presence of lower melting point phases in the precursor allows for the initiation of kesterite formation in the early stages of the annealing process and contributes to the formation of high-quality kesterite absorbers as the temperature increases during annealing. The aim of this study is to compare the formation mechanisms of ACZTS materials during the final annealing stages (475–550 °C) for both protocols, the commonly used Cu^{2+} and Sn^{2+} protocol and the recently developed Cu^{+} and Sn^{4+} approach, which have shown potential for producing highly efficient kesterite solar cells. While previous studies have explored the influence of Sn and Cu oxidation states on kesterite materials, they have focused primarily on CZTSSe compounds, which are produced through a selinization process and exhibit narrow bandgaps [15]. In contrast, this study examines the transformation of all absorbers into sulfurized CZTS, an approach that remains underexplored for large-bandgap CZTS absorbers. For this purpose, we annealed as-deposited Sol-1 and Sol-2 at temperatures ranging from 475 to 550 °C. A combination of XRD, Raman spectroscopy, SEM, and EDX analyses was used to investigate how the oxidation states of the metal precursors affect the properties of the final CZTS thin films at high annealing temperatures. These complementary techniques provide a comprehensive understanding of the influence of metal precursor chemistry on kesterite phase formation, crystallinity, morphology, and elemental distribution, ultimately offering insights into how oxidation states control the quality of CZTS absorbers during the sulfurization process.

Figure 5 shows the XRD patterns of the CZTS absorbers prepared with Sol-1 and Sol-2 and annealed at different temperatures. All samples exhibit similar peaks at the (112), (200), (220), and (312) diffraction planes of the polycrystalline kesterite phase (JCPDS #026-0575), indicating the formation of crystalline kesterite phases even at lower annealing temperatures (e.g., 475 °C). However, the shape and intensity of the main diffraction peaks vary significantly with changes in the annealing temperature between the two samples.

At the lowest temperature of 475 °C, the sample prepared with Sol-1 shows SnS_2 diffraction peaks, along with the disappearance of the SnS peak, indicating partial conversion of SnS to SnS_2. This conversion becomes more pronounced as the temperature increases to 500 °C, with a highly intense peak at 15° corresponding to the (000) diffraction peak of the SnS_2 phase [28]. This peak is even more intense than the (112) plane of the kesterite phase, likely due to the sensitivity of the SnS_2 phase to XRD analysis. However, this peak disappears after increasing the temperature to 525 °C and 550 °C, which may indicate that at higher temperatures, SnS_2 participates in the formation of kesterite phases by interacting with other Cu- and Zn-based phases. Small traces of SnS_2 are still observed at these temperatures, suggesting that complete fusion of SnS_2 with CZTS is difficult to

achieve. At 550 °C, the principal peak of the kesterite phase is narrower and more intense, indicating higher crystallinity. The XRD results were also confirmed via Raman spectroscopy with 532 nm and 785 nm excitation wavelengths. The Raman spectra obtained at 532 nm for Sol-1 confirm the formation of the kesterite phase at lower temperatures, which is consistent with the XRD results. However, some peaks corresponding to Cu_2S at 480 cm^{-1} [29] and ZnS at 680 cm^{-1} are present. The Cu_2S phases become more pronounced as the temperature increases, possibly because of diffusion to the top of the absorber at higher temperatures or the transformation of CuS to Cu_2S, which then reacts with SnS_2 and ZnS to form kesterite materials [20,30]. At 550 °C, all these phases disappear, except for small traces of ZnS, likely due to the Zn-rich stoichiometry used. The near-resonance Raman spectra with 785 nm excitation, presented in Figure 6a, show that as the temperature increases, the sharpness and intensity of the S–S interaction peaks improve, indicating a more ordered matrix, which is in line with the XRD results. Atomic disorder in the kesterite phase is influenced by several factors, including the presence of secondary phases, which results in an inhomogeneous distribution of atoms and a disordered matrix. At higher annealing temperatures, the transformation of some secondary phases into kesterite materials leads to a more ordered and less defective matrix.

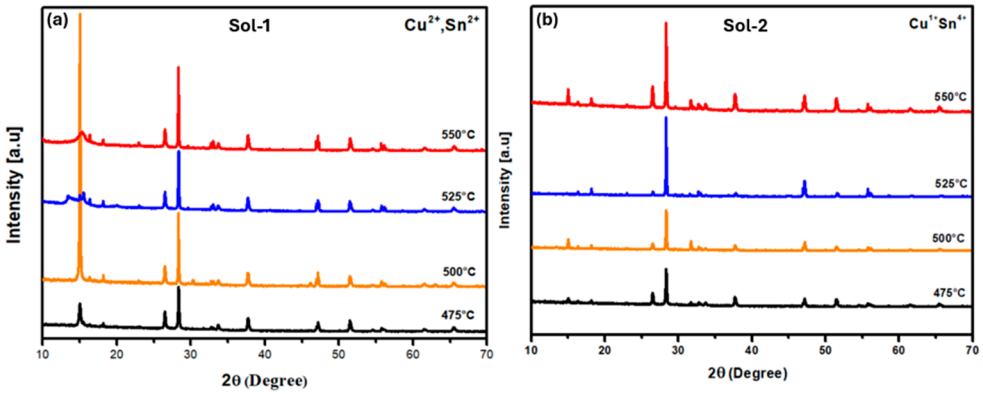

Figure 5. XRD patterns of CZTS thin-film absorbers prepared with Sol-1 (**a**) and Sol-2 (**b**) and annealed at different temperatures.

A completely different behavior is observed during the growth mechanism of kesterite materials prepared using Sol-2. The XRD results in Figure 6b show the formation of the kesterite phase at lower temperatures, similar to the sample prepared using Sol-1. However, some traces of SnS_2 are observed, likely due to the excess Sn^{4+} used in the solution. Notably, SnS_2 can appear in XRD patterns even when it is present in small amounts. This phase disappears in the sample annealed at 525 °C, but when the temperature is increased to 550 °C, SnS_2 reappears along with some other phases, possibly due to the decomposition of kesterite at higher temperatures, as reported in previous works. The Raman spectra also confirmed these results, showing the appearance of peaks corresponding to secondary phases in the Raman curve obtained at 532 nm for the sample annealed at 550 °C and a reduced intensity with broad peaks in the spectrum obtained at 785 nm. These findings support the direct transformation from an amorphous to a highly crystalline kesterite phase during the annealing process. However, the early formation of kesterite phases during the initial stages of annealing may lead to the decomposition of kesterite into secondary phases at higher temperatures. The surface SEM images presented in Figure 7 reveal significant differences in grain formation and distribution across the temperature range. For samples prepared with Sol-2, incomplete grain formation and the presence of numerous cracks are observed at 475 °C. Increasing the annealing temperature to 500 °C promoted the development of CZTS grains, with the emergence of larger grains, possibly corresponding to secondary phases such as SnS_2, as indicated by the XRD results. At temperatures above 500 °C, the grain size improved, and the grain distribution became more homogeneous, particularly in samples annealed at 550 °C.

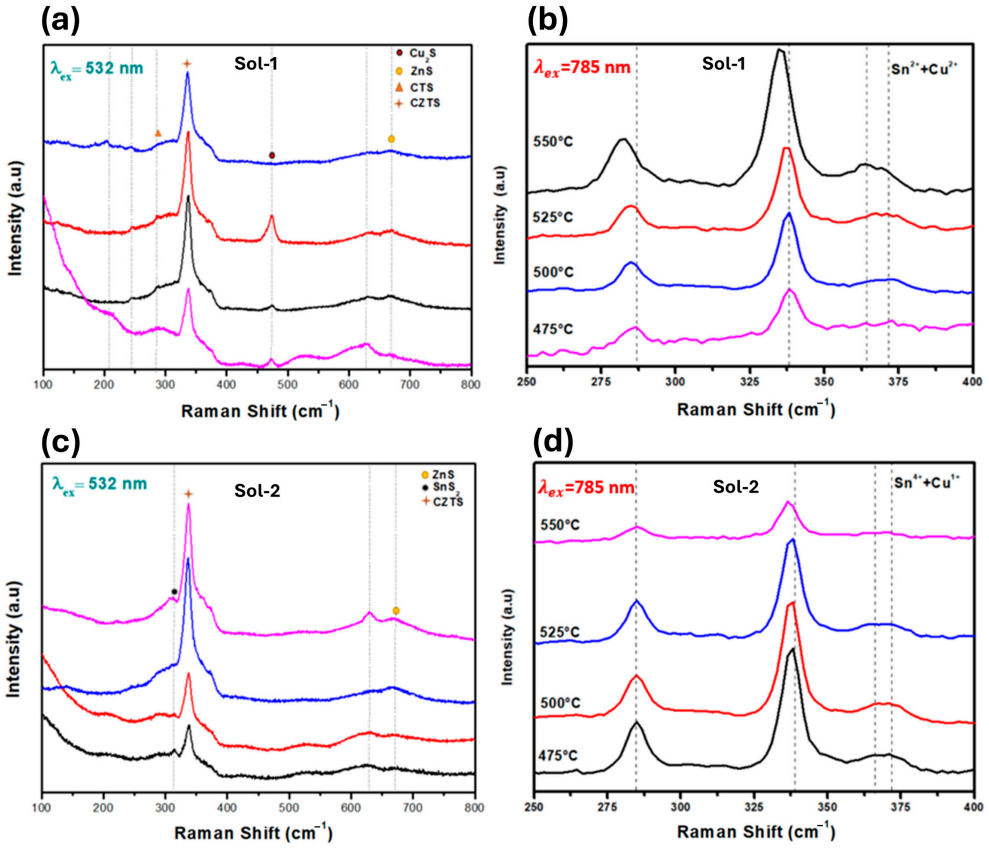

Figure 6. Raman spectra of CZTS absorbers prepared with Sol-1 and Sol-2 and annealed at different temperatures, recorded with excitation wavelengths of 532 (**a**,**c**) and 785 nm (**b**,**d**).

For the samples prepared with Sol-1, crystalline CZTS nanoparticles begin to form at 475 °C. A further increase in the annealing temperature to 525 °C enhances the morphology and promotes greater grain growth. At 550 °C, the appearance of larger grains may be associated with the formation of secondary phases, potentially due to the partial decomposition of the kesterite phase, as suggested by previous characterizations.

In general, both protocols lead to the formation of high-quality kesterite materials after the annealing process; however, the formation pathway and evolution were different between the two protocols, and each protocol requires annealing at their optimized temperature. During the annealing process, the transformation from precursor to absorber CZTS formation differs significantly between protocols using Cu^{2+} and Sn^{2+} (Sol-1) and those using Cu^{+} and Sn^{4+} (Sol-2). Figure 8 summarizes the transformation mechanisms from solution to precursor and from precursor to absorber for Sol-1 and Sol-2. In Sol-1, where Cu^{2+} and Sn^{2+} are employed, CZTS has two pathways of formation. The first initially forms an amorphous phase and then converts to crystalline CZTS. The second pathway is accompanied by the formation of ZnS, CuS, and SnS, which transform into SnS_2 as a secondary phase. As annealing progresses, these secondary phases fuse to form a crystalline CZTS structure. Conversely, in Sol-2, which uses Cu^{+} and Sn^{4+}, one pathway involves the early crystallization of CZTS with minimal secondary phase formation. This results in a nearly single-phase CZTS structure with superior crystallinity at lower temperatures. At higher annealing temperatures, these materials decompose.

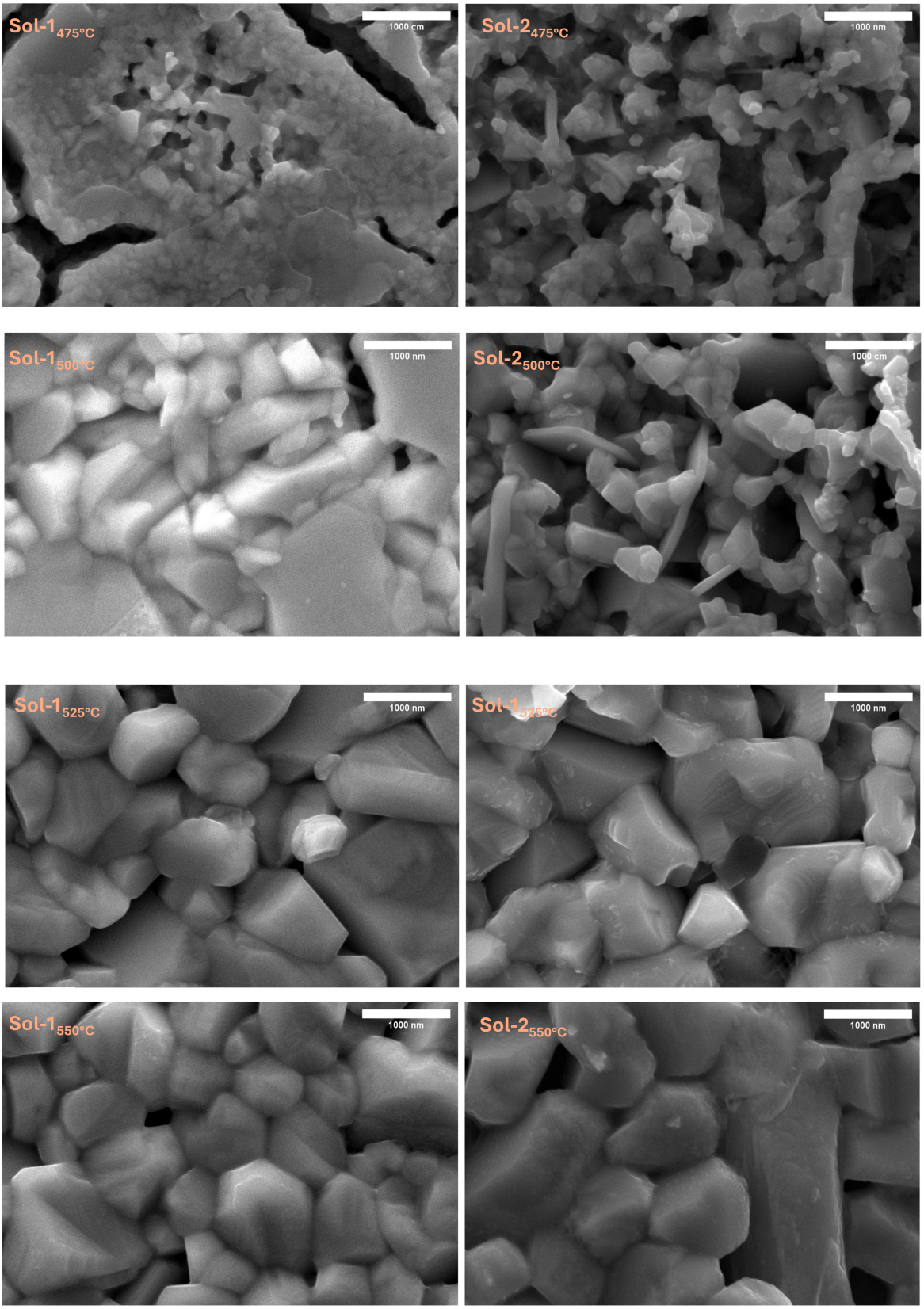

Figure 7. Surface SEM images of CZTS absorbers prepared with Sol-1 and Sol-2 and annealed at different temperatures.

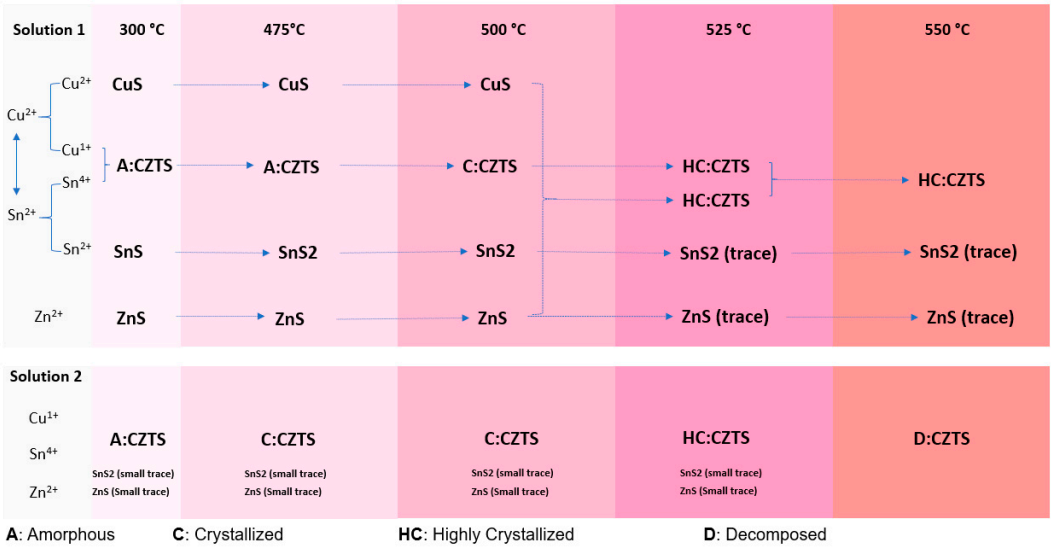

Figure 8. Transformation mechanisms from the solution to the precursor and from the precursor to the absorber for Sol-1 and Sol-2.

4. Conclusions

In this study, we successfully synthesized Ag-alloyed CZTS absorbers via the sol–gel method on a transparent FTO back electrode, with a focus on exploring the effects of different oxidation states of copper (Cu) and tin (Sn) precursors. The results of our analysis demonstrated that the oxidation state of metal ions significantly influences the morphological and structural properties of kesterite materials. This control has the potential to enhance their optoelectronic properties, leading to improved performance when utilized in solar cell applications. X-ray diffraction and Raman spectroscopy confirmed the formation of kesterite structures with minimal secondary phases, whereas SEM analyses further highlighted the impact of precursor oxidation states on the surface morphology, crystallinity, and grain size of the films. The findings from this work underscore the importance of precursor chemistry in the sol–gel synthesis of kesterite materials and highlight a promising approach for optimizing the performance of Ag-alloyed CZTS. By utilizing molecular inks and carefully controlling the oxidation states of metal precursors, this study paves the way for more efficient and scalable methods for producing high-quality kesterite absorbers, with implications for advancing the development of low-cost, sustainable thin-film solar cell technologies. Despite the growing importance of solution engineering in kesterite materials prepared using the sol–gel method, the majority of studies have focused on the precursor thin films and the annealing process, with a notable lack of information regarding the solution phase. This work, along with several previous studies, has demonstrated the critical importance of controlling the solution preparation process in order to produce a high-quality kesterite absorber. It would be beneficial for future research to focus on the solution preparation and to analyze the process from the solution phase. This approach could lead to a deeper understanding and greater control over the growth of kesterite materials, which in turn could facilitate the fabrication of more efficient solar cells.

Author Contributions: Conceptualization, N.E., Y.C. and A.E.; methodology, A.E., N.E. and Y.C.; validation, A.E., N.E., Y.C. and Z.S.; formal analysis, N.E., A.E. and Y.C.; investigation, N.E. and Z.S.; resources, Z.S.; data curation, A.E. and N.E.; writing—original draft preparation, N.E., Y.C., A.E. and Z.S.; writing—review and editing, N.E., Y.C., A.E. and Z.S.; visualization, Z.S.; supervision, Z.S.; project administration, Z.S.; funding acquisition, Z.S. All authors have read and agreed to the published version of the manuscript.

Funding: This research was funded by the European Union's Horizon 2020 research and innovation program under grant agreement No. 777968 (INFINITE-CELL project).

Data Availability Statement: All the data will be shared upon request.

Acknowledgments: The authors would like to thank Othman el Khouja for Raman analysis.

Conflicts of Interest: The authors declare that they have no known competing financial interests or personal relationships that could have appeared to influence the work reported in this paper.

References

1. Miccoli, I.; Prete, P.; Marzo, F.; Cannoletta, D.; Lovergine, N. Synthesis of Vertically-aligned GaAs Nanowires on GaAs/(111)Si Hetero-substrates by Metalorganic Vapour Phase Epitaxy. *Cryst. Res. Technol.* **2011**, *46*, 795–800. [CrossRef]
2. Di Carlo, V.; Prete, P.; Dubrovskii, V.G.; Berdnikov, Y.; Lovergine, N. CdTe Nanowires by Au-Catalyzed Metalorganic Vapor Phase Epitaxy. *Nano Lett.* **2017**, *17*, 4075–4082. [CrossRef]
3. Dang, H.; Ososanaya, E.; Zhang, N. Improving Reliability of Window-Absorber Solar Cells through CdS Nanowires. *Opt. Mater.* **2022**, *132*, 112721. [CrossRef]
4. Larramona, G.; Choné, C.; Meissner, D.; Ernits, K.; Bras, P.; Ren, Y.; Martín-Salinas, R.; Rodríguez-Villatoro, J.L.; Vermang, B.; Brammertz, G. Stability, Reliability, Upscaling and Possible Technological Applications of Kesterite Solar Cells. *J. Phys. Energy* **2020**, *2*, 024009. [CrossRef]
5. Engberg, S.; Martinho, F.; Gansukh, M.; Protti, A.; Küngas, R.; Stamate, E.; Hansen, O.; Canulescu, S.; Schou, J. Spin-Coated Cu_2ZnSnS_4 Solar Cells: A Study on the Transformation from Ink to Film. *Sci. Rep.* **2020**, *10*, 20749. [CrossRef] [PubMed]
6. Moreno-Regino, V.D.; Castanedo-Pérez, R.; Márquez-Marín, J.; Torres-Delgado, G. Cu_2ZnSnS_4 Films Properties Deposited by Spray Pyrolysis, Subjected to a Combined Novel Thermal Treatment: CSS Sulfurization and RTA Post-Treatment. *J. Alloys Compd.* **2023**, *956*, 170379. [CrossRef]
7. Katirci, R.; Onel, M.N.; Danaci, I.; Danaci, K.I.; Ozbay, S.; Erden, F. Fabrication of CZTS Films through a Combined Electrodeposition and Solution Process: An Experimental and First-Principles Study. *ChemElectroChem* **2023**, *10*, e202300162. [CrossRef]
8. Simya, O.K.; Geetha Priyadarshini, B.; Balachander, K.; Ashok, A.M. Formation of a Phase Pure Kesterite CZTSe Thin Films Using Multisource Hybrid Physical Vapour Deposition. *Mater. Res. Express* **2020**, *7*, 016419. [CrossRef]
9. Wang, W.; Winkler, M.T.; Gunawan, O.; Gokmen, T.; Todorov, T.K.; Zhu, Y.; Mitzi, D.B. Device Characteristics of CZTSSe Thin-Film Solar Cells with 12.6% Efficiency. *Adv. Energy Mater.* **2014**, *4*, 1301465. [CrossRef]
10. Li, Y.; Cui, C.; Wei, H.; Shao, Z.; Wu, Z.; Zhang, S.; Wang, X.; Pang, S.; Cui, G. Suppressing Element Inhomogeneity Enables 14.9% Efficiency CZTSSe Solar Cells. *Adv. Mater.* **2024**, *36*, 2400138. [CrossRef] [PubMed]
11. Shin, S.W.; Pawar, S.M.; Park, C.Y.; Yun, J.H.; Moon, J.-H.; Kim, J.H.; Lee, J.Y. Studies on Cu_2ZnSnS_4 (CZTS) Absorber Layer Using Different Stacking Orders in Precursor Thin Films. *Sol. Energy Mater. Sol. Cells* **2011**, *95*, 3202–3206. [CrossRef]
12. Patel, S.B.; Gohel, J.V. Effect of Type of Solvent on the Sol-Gel Spin Coated CZTS Thin Films. *PAIJ* **2017**, *1*, 126–129. [CrossRef]
13. Kumar, Y.B.K.; Bhaskar, P.U.; Babu, G.S.; Raja, V.S. Effect of Copper Salt and Thiourea Concentrations on the Formation of Cu_2ZnSnS_4 Thin Films by Spray Pyrolysis. *Phys. Status Solidi (A)* **2010**, *207*, 149–156. [CrossRef]
14. Moser, S.; Krummenacher, J.; Aribia, A.; Morzy, J.; Carron, R. Mitigating Sn Loss via Anion Substitution in the Cu^{2+}–Sn^{2+} Precursor System for $Cu_2ZnSn(S, Se)_4$ Solar Cells. *J. Mater. Chem. A* **2024**, *12*, 32424–32435. [CrossRef]
15. Li, Q.; Sun, S.; Li, X.; Li, X.; Liu, X.; Zhang, D.; Yu, N.; Wang, S. Influence of the Oxidation State of Sn in the Precursor and Selenization Temperature on $Cu_2ZnSn(S,Se)_4$ Thin Film Solar Cells. *Mater. Sci. Semicond. Process.* **2022**, *138*, 106251. [CrossRef]
16. Agbenyeke, R.; Sheppard, A.; Keynon, J.; Benhaddou, N.; Fleck, N.; Corsetti, V.; Alkhalifah, M.A.; Tiwari, D.; Bowers, J.W.; Fermin, D.J. Correlating Molecular Precursor Interactions with Device Performance in Solution-Processed $Cu_2ZnSn(S,Se)_4$ Thin-Film Solar Cells. ACS Appl. *Mater. Interfaces* **2024**, *16*, 35315–35322. [CrossRef]
17. Gong, Y.; Zhang, Y.; Zhu, Q.; Zhou, Y.; Qiu, R.; Niu, C.; Xin, H. Identify the Origin of the V_{oc} Deficit of Kestertie Solar Cells from the Two Reaction Paths Induced by Sn^{2+} and Sn^{4+} Precursors in DMSO Solution. In Proceedings of the 2021 IEEE 48th Photovoltaic Specialists Conference (PVSC), Fort Lauderdale, FL, USA, 20–25 June 2021; pp. 1995–1997.
18. Xin, H.; Katahara, J.K.; Braly, I.L.; Hillhouse, H.W. 8% Efficient $Cu_2ZnSn(S,Se)_4$ Solar Cells from Redox Equilibrated Simple Precursors in DMSO. *Adv. Energy Mater.* **2014**, *4*, 1301823. [CrossRef]
19. Todorov, T.; Hillhouse, H.W.; Aazou, S.; Sekkat, Z.; Vigil-Galán, O.; Deshmukh, S.D.; Agrawal, R.; Bourdais, S.; Valdés, M.; Arnou, P.; et al. Solution-Based Synthesis of Kesterite Thin Film Semiconductors. *J. Phys. Energy* **2020**, *2*, 012003. [CrossRef]
20. Gong, Y.; Zhang, Y.; Zhu, Q.; Zhou, Y.; Qiu, R.; Niu, C.; Yan, W.; Huang, W.; Xin, H. Identifying the Origin of the V_{oc} Deficit of Kesterite Solar Cells from the Two Grain Growth Mechanisms Induced by Sn^{2+} and Sn^{4+} Precursors in DMSO Solution. *Energy Environ. Sci.* **2021**, *14*, 2369–2380. [CrossRef]
21. Su, Z.; Sun, K.; Han, Z.; Cui, H.; Liu, F.; Lai, Y.; Li, J.; Hao, X.; Liu, Y.; Green, M.A. Fabrication of Cu_2ZnSnS_4 Solar Cells with 5.1% Efficiency via Thermal Decomposition and Reaction Using a Non-Toxic Sol–Gel Route. *J. Mater. Chem. A* **2014**, *2*, 500–509. [CrossRef]
22. Gong, Y.; Zhang, Y.; Jedlicka, E.; Giridharagopal, R.; Clark, J.A.; Yan, W.; Niu, C.; Qiu, R.; Jiang, J.; Yu, S.; et al. Sn4+ Precursor Enables 12.4% Efficient Kesterite Solar Cell from DMSO Solution with Open Circuit Voltage Deficit below 0.30 V. *Sci. China Mater.* **2021**, *64*, 52–60. [CrossRef]

23. Ahmoum, H.; Chelvanathan, P.; Su'ait, M.S.; Boughrara, M.; Li, G.; Gebauer, R.; Sopian, K.; Kerouad, M.; Amin, N.; Wang, Q. Sol-Gel Prepared Cu_2ZnSnS_4 (CZTS) Semiconductor Thin Films: Role of Solvent Removal Processing Temperature. *Mater. Sci. Semicond. Process.* **2021**, *132*, 105874. [CrossRef]
24. Scragg, J.J.S.; Choubrac, L.; Lafond, A.; Ericson, T.; Platzer-Björkman, C. A Low-Temperature Order-Disorder Transition in Cu_2ZnSnS_4 Thin Films. *Appl. Phys. Lett.* **2014**, *104*, 041911. [CrossRef]
25. Avendaño, C.A.M.; Mathews, N.R.; Pal, M.; Delgado, F.P.; Mathew, X. Structural Evolution of Multilayer SnS/Cu/ZnS Stack to Phase-Pure Cu_2ZnSnS_4 Thin Films by Thermal Processing. *ECS J. Solid State Sci. Technol.* **2015**, *4*, P91–P96. [CrossRef]
26. Su, C.-Y.; Chiu, C.-Y.; Ting, J.-M. Cu_2ZnSnS_4 Absorption Layers with Controlled Phase Purity. *Sci. Rep.* **2015**, *5*, 9291. [CrossRef]
27. Zhou, J.; Xu, X.; Wu, H.; Wang, J.; Lou, L.; Yin, K.; Gong, Y.; Shi, J.; Luo, Y.; Li, D.; et al. Control of the Phase Evolution of Kesterite by Tuning of the Selenium Partial Pressure for Solar Cells with 13.8% Certified Efficiency. *Nat. Energy* **2023**, *8*, 526–535. [CrossRef]
28. Kim, C.; Hong, S. Effects of Cu^+ Ion Implantation on Band Gap and Raman Shift of Cu_2ZnSnS_4 Thin Films. *Curr. Appl. Phys.* **2023**, *50*, 153–160. [CrossRef]
29. Yu, S.M.; Lim, K.-S.; Shin, D.-W.; Oh, T.-S.; Yoo, J.-B. Effect of the Intermediate Sulfide Layer on the Cu_2ZnSnS_4-Based Solar Cells. *J. Mater. Sci. Mater. Electron.* **2017**, *28*, 5696–5702. [CrossRef]
30. Jung, H.R.; Shin, S.W.; Suryawanshi, M.P.; Yeo, S.J.; Yun, J.H.; Moon, J.H.; Kim, J.H. Phase Evolution Pathways of Kesterite Cu_2ZnSnS_4 and $Cu_2ZnSnSe_4$ Thin Films during the Annealing of Sputtered Cu-Sn-Zn Metallic Precursors. *Sol. Energy* **2017**, *145*, 2–12. [CrossRef]